

Three-dimensional topological insulators in the octahedron-decorated cubic lattice

Jing-Min Hou,* Wen-Xin Zhang, and Guo-Xiang Wang
Department of Physics, Southeast University, Nanjing, 211189, China
 (Dated: November 11, 2018)

We investigate a tight-binding model of the octahedron-decorated cubic lattice with spin-orbit coupling. We calculate the band structure of the lattice and evaluate the Z_2 topological indices. According to the Z_2 topological indices and the band structure, we present the phase diagrams of the lattice with different filling fractions. We find that the (1;111) and (1;000) strong topological insulators occur in some range of parameters at 1/6, 1/2 and 2/3 filling fractions. Additionally, the (0;111) weak topological insulator is found at 1/6 and 2/3 filling fractions. We analyze and discuss the characteristics of these topological insulators and their surfaces states.

PACS numbers: 73.43.-f, 71.10.Fd, 73.20.-r, 72.25.-b

I. INTRODUCTION

Usually, different phases of matter can be classified using Landau's approach according to their underlying symmetries[1]. In 1980s, the discovery of the quantum Hall effect changed physicists' viewpoint on the classification of matter[2]. The quantum Hall states can be classified by a topological invariant, now named the TKNN number[3] (equivalent to the first Chern number), which is directly connected to the quantized Hall conductivity, but they have the same symmetry. Since the Hall conductivity is odd under time reversal, the topological non-trivial quantum Hall states can only occur when time reversal symmetry is broken, which is performed by a magnetic field. In 1988, Haldane also proposed a time reversal symmetry broken toy model without a magnetic field to realize quantum Hall states[4]. All the quantum Hall states have a gapped band structure in bulk and chiral gapless edge states that are topologically protected.

Recently, the promising prospect of spintronics in technology stimulates physicists to generate spin current. Quantum spin Hall effect was proposed to create spin current[5, 6]. The quantum spin Hall states are non-trivial topological phases with time reversal symmetry, which have a bulk gap and topologically protected gapless helical edge states. For the above reason, the quantum spin Hall states also called topological insulators. Two-dimensional topological insulators are characterized by a Z_2 topological index $\nu = 0, 1$ [7]. For a non-trivial topological insulator the topological index has a value $\nu = 1$ while $\nu = 0$ for a trivial band insulator. Therefore, a topological insulator always has a metallic boundary when placed next to a vacuum or an ordinary band insulator because topological invariants cannot change as long as a material remains insulating. The remarkable metallic boundaries of topological insulators may result in new spintronic or magnetoelectric devices and a new architecture for topological quantum bits. In quantum spin Hall phases, the spin-orbit coupling plays

the role of the spin-dependent effective magnetic field. The first real material, a HgTe quantum well, supporting two-dimensional topological insulators was predicted by Bernevig, *et al.*[8] and experimentally conformed by König *et al.*[9].

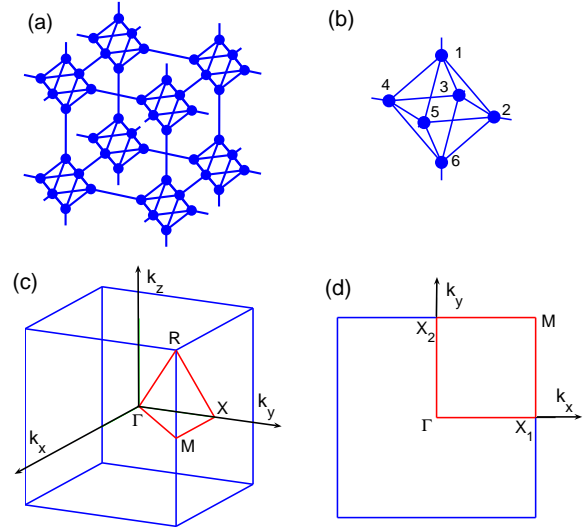


FIG. 1: (Color online). (a) The octahedron-decorated cubic lattice which can be obtained by replacing every lattice site of a cubic lattice with an octahedral cluster as shown in (b). (c) The three-dimensional Brillouin zone and high symmetry points. (d) The two-dimensional Brillouin zone of a slab with two 001 surfaces.

Soon after the quantum spin Hall insulator was discovered, time-reversal invariant topological insulators were generalized to three dimensions[10–12]. Three-dimensional time-reversal invariant band insulators are classified according to four Z_2 topological indices ($\nu_0; \nu_1\nu_2\nu_3$) with $\nu_i = 0, 1$ [10]. In three dimensions, the time-reversal invariant band insulators can be classified into 16 phases according to the four Z_2 topological indices. A band insulator with $\nu_0 = 1$ is called a strong topological insulator(STI), a band insulator with

*Electronic address: jmhou@seu.edu.cn

$\nu_0 = 0$ and at least one non-zero $\nu_i (i = 1, 2, 3)$ is called a weak topological insulator (WTI), while an ordinary trivial band insulator has an index (0;000). For an STI phase, the surface states have an odd number of Dirac points, which are topologically protected and for a WTI or trivial band insulator phase, the surface states have an even number of Dirac points. Fu and Kane firstly predicted that $\text{Bi}_{1-x}\text{Sb}_x$ supports a three-dimensional topological insulator[13], which was conformed experimentally by Hsieh, *et al.* in 2008[14]. Later, Bi_2Te_3 was discovered to be a three-dimensional insulator experimentally as a second generation material[15], which also was supported by theoretical calculations[15, 16]. Additionally, reference [16] also predicted that Bi_2Te_3 and Sb_2Te_3 are second generation materials supporting three-dimensional topological insulators. The later experimental studies on Bi_2Te_3 [17–19] and Sb_2Te_3 [19] identified their topological band structures.

To help experimental physicists find more topological insulator materials, theoretical physicists have investigated several models that support non-trivial topological insulators. Theoretical studies have demonstrated that, within the tight-binding approximation and with the spin-orbit coupling, the honeycomb[6], kagome[20], checkerboard[21], decorated honeycomb[22], Lieb[23], and square-octagon[24] lattices support two-dimensional topological insulators and the diamond[10], pyrochlore[25], and perovskite[23] lattices support three-dimensional topological insulators.

In this paper, we shall show that a new lattice, the octahedron-decorated cubic lattice as shown in Fig.1 (a), supports three-dimensional topological insulators with the spin-orbit coupling existing. This lattice can be regarded as a three-dimensional generalization of the square-octagon lattice[22]. We find that this model supports STI and WTI phases for 1/6 and 2/3 filling and STI phases for 1/2 filling as well as ordinary band insulator and metal phases.

II. MODEL

We consider the octahedron-decorated cubic lattice as shown in Fig.1 (a), which can be obtained by replacing every lattice site of a cubic lattice with an octahedral cluster as shown in Fig.1(b). This lattice has a unit cell with six different lattice sites as denoted in Fig.1(b) so that it contains six sublattices. Here, we assume that the distance between the centers of two nearest-neighbor octahedral clusters is a , which is the same with the lattice constant of all sublattices, the distance of every lattice site of an octahedral cluster from its center is $a/4$, and the distance of two nearest-neighbor lattice sites in different octahedral clusters is $a/2$. With the tight-binding approximation, we can write the second quantized Hamil-

tonian of the lattice as follows,

$$H_0 = -t \sum_{\langle i,j \rangle, \sigma} c_{i\sigma}^\dagger c_{j\sigma} - t_1 \sum_{[i,j], \sigma} c_{i\sigma}^\dagger c_{j\sigma} \quad (1)$$

where $c_{i\sigma}$ is the annihilation operator destructing an electron with spin σ on the site \mathbf{r}_i of the octahedron-decorated cubic lattice, $\langle i, j \rangle$ represents nearest-neighbor hopping in the same octahedral cluster with amplitude t and $[i, j]$ denotes nearest-neighbor hopping between two different octahedral clusters with amplitude t_1 .

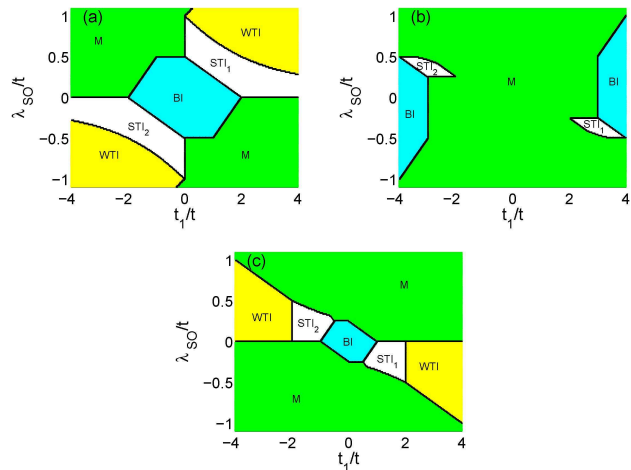


FIG. 2: (Color online). Phase diagrams of the octahedron-decorated cubic lattice for (a) 1/6 filling, (b) 1/2 filling, and (c) 2/3 filling. Here, BI denotes a trivial band insulator; STI_1 and STI_2 denote (1; 111) and (1; 000) strong topological insulators, respectively; WTI denotes a (0; 111) weak topological insulator; and M denotes a metal phase.

In momentum space, the Hamiltonian (1) can be represented by $H_0 = \sum_{\mathbf{k}\sigma} \Psi_{\mathbf{k}\sigma}^\dagger \mathcal{H}_{\mathbf{k}}^{(0)} \Psi_{\mathbf{k}\sigma}$ with $\Psi_{\mathbf{k}\sigma} = (c_{1\mathbf{k}\sigma}, c_{2\mathbf{k}\sigma}, c_{3\mathbf{k}\sigma}, c_{4\mathbf{k}\sigma}, c_{5\mathbf{k}\sigma}, c_{6\mathbf{k}\sigma})^T$, which are ordered according to the sequence denoted in Fig.1(b). Here, $\mathcal{H}_{\mathbf{k}}^{(0)}$ takes the following form,

$$\mathcal{H}_{\mathbf{k}}^0 = \begin{pmatrix} 0 & t & t & t & t & t_1 e^{ik_z} \\ t & 0 & t & t_1 e^{ik_x} & t & t \\ t & t & 0 & t & t_1 e^{ik_y} & t \\ t & t_1 e^{-ik_x} & t & 0 & t & t \\ t & t & t_1 e^{-ik_y} & t & 0 & t \\ t_1 e^{-ik_z} & t & t & t & t & 0 \end{pmatrix} \quad (2)$$

Since H_0 is spin-decoupling, $\mathcal{H}_{\mathbf{k}}^0$ is spin-independent, i.e. it is the same for both spin-up and spin-down electrons. Fig.1(c) shows the first Brillouin zone of the octahedron-decorated cubic lattice. The spectrum of Eq.(2) with $t_1 = t$ is calculated and shown in Fig.3(d). The spectrum contains six bands which come from the six sites in every unit cell. A gap exists between the first and second bands. The second, third and fourth bands touch

together at points Γ, R and M . The third, fourth and fifth band touch at point X , near which a Dirac cone occurs. Five bands including the second, third, fourth, fifth and sixth bands meet at point Γ . Along the $\Gamma \rightarrow R$ line in momentum space, the second and third bands are degenerate and the fifth and sixth bands are degenerate.

Now, in order to find non-trivial topological insulators in the octahedron-decorated cubic lattice, we proceed to introduce the spin-orbit interactions between next-nearest-neighbor sites as follows,

$$H_{\text{SO}} = i \frac{8\lambda_{\text{SO}}}{a^2} \sum_{\langle\langle i,j \rangle\rangle} (\mathbf{d}_{ij}^1 \times \mathbf{d}_{ij}^2) \cdot \boldsymbol{\sigma}_{\alpha\beta} c_{i\alpha}^\dagger c_{j\beta},$$

where $\langle\langle i,j \rangle\rangle$ represents two next-nearest-neighbor sites i, j , and λ_{SO} is the amplitude of spin-orbit coupling of the two next-nearest-neighbor sites. $\boldsymbol{\sigma} = (\sigma_x, \sigma_y, \sigma_z)$ is the vector of Pauli spin matrices. $\mathbf{d}_{ij}^{1,2}$ are the two nearest neighbor bond vectors traversed between sites i and j with $8|\mathbf{d}_{ij}^1 \times \mathbf{d}_{ij}^2|/a^2 = 1$. In momentum space, the Hamiltonian for spin-orbit coupling (3) can be expressed as $H_{\text{SO}} = \sum_{\mathbf{k}} \Psi_{\mathbf{k}}^\dagger \mathcal{H}_{\mathbf{k}}^{\text{SO}} \Psi_{\mathbf{k}}$ with $\Psi_{\mathbf{k}} = (c_{1\mathbf{k}\uparrow}, c_{2\mathbf{k}\uparrow}, c_{3\mathbf{k}\uparrow}, c_{4\mathbf{k}\uparrow}, c_{5\mathbf{k}\uparrow}, c_{6\mathbf{k}\uparrow}, c_{1\mathbf{k}\downarrow}, c_{2\mathbf{k}\downarrow}, c_{3\mathbf{k}\downarrow}, c_{4\mathbf{k}\downarrow}, c_{5\mathbf{k}\downarrow}, c_{6\mathbf{k}\downarrow})^T$. Since $\mathcal{H}_{\mathbf{k}}^{\text{SO}}$ does not decouple for the two spin projections, it is a 12×12 matrix. In momentum space, the total single particle Hamiltonian is $\mathcal{H}_{\mathbf{k}} = \mathcal{H}_{\mathbf{k}}^0 + \mathcal{H}_{\mathbf{k}}^{\text{SO}}$. The bands and eigenstates can be obtained by exactly diagonalizing $\mathcal{H}_{\mathbf{k}}$.

III. THREE-DIMENSIONAL TOPOLOGICAL INSULATORS

The classification of three-dimensional topological insulators is presented in Ref.[10]. For three-dimensional lattices there eight distinct time reversal invariant momenta (TRIM), which can be expressed in terms of primitive reciprocal lattice vectors as $\Gamma_{i=(n_1, n_2, n_3)} = (n_1 \mathbf{b}_1 + n_2 \mathbf{b}_2 + n_3 \mathbf{b}_3)/2$ with $n_j = 0, 1$. Three-dimensional topological insulators can be distinguished by four Z_2 topological invariants $(\nu_0; \nu_1 \nu_2 \nu_3)$, which are defined as $(-1)^{\nu_0} = \prod_{n_j=0,1} \delta_{n_1 n_2 n_3}$ and $(-1)^{\nu_i} = \prod_{n_j \neq i=0,1; n_i=1} \delta_{n_1 n_2 n_3}$, where $\delta_{n_1 n_2 n_3} = \sqrt{\det[w(\Gamma_{n_1 n_2 n_3})]} / \text{Pf}[w(\Gamma_{n_1 n_2 n_3})] = \pm 1$. Here the unitary matrix w is defined as $w_{ij}(\mathbf{k}) = \langle u_i(-\mathbf{k}) | \Theta | u_j(\mathbf{k}) \rangle$ with Θ being the time reversal operator and $|u_j(\mathbf{k})\rangle$ being the Bloch wave functions for occupied bands. Fu and Kane have found a simple method to identify the Z_2 invariants for the system with the presence of inversion symmetry[13]. In this case, $\delta_{n_1 n_2 n_3}$ can be calculated by $\delta_{n_1 n_2 n_3} = \prod_{m=1}^N \xi_{2m}(\Gamma_{n_1 n_2 n_3})$, where N is the number of occupied bands and $\xi_{2m}(\Gamma_{n_1 n_2 n_3}) = \pm 1$ is the parity eigenvalue of the $2m$ th occupied band at $\Gamma_{n_1 n_2 n_3}$. Our model is inversion symmetric so we will adopt this method to evaluate the Z_2 invariants $\nu_i (i = 0, 1, 2, 3)$. We select the center of an octahedron in the lattice as the center of inversion, then the parity operator

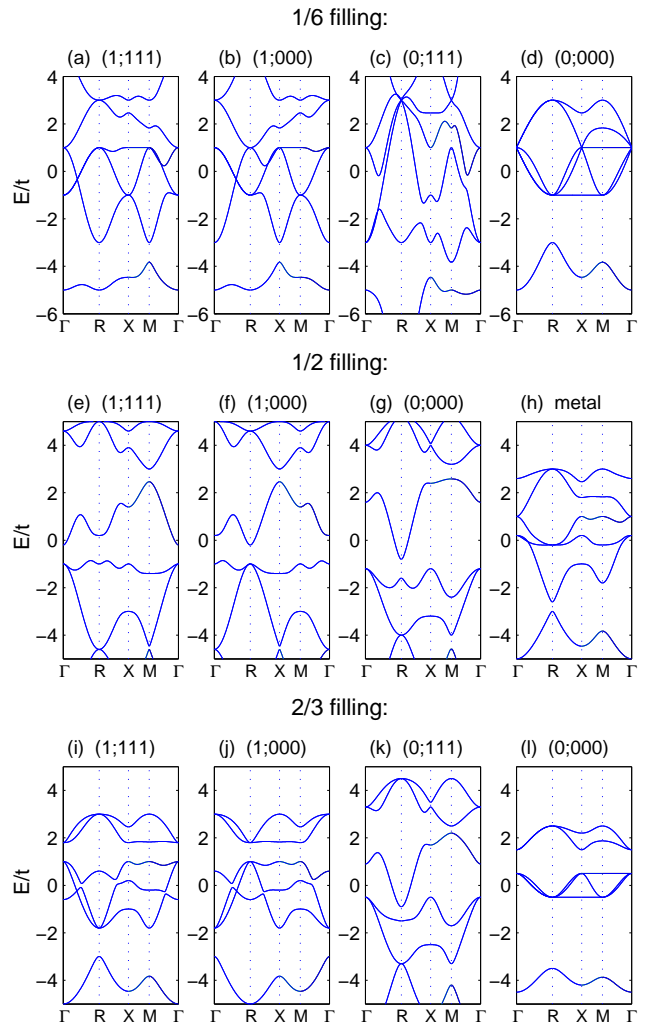


FIG. 3: (Color online). Band structures of the octahedron-decorated cubic lattice for various parameters t_1 and λ_{SO} . Here, the horizontal axis represents the wave vectors along the path in the first Brillouin zone indicated by the red lines in Fig.1(c). (a) $t_1 = t, \lambda_{\text{SO}} = 0.5t$, (b) $t_1 = -t, \lambda_{\text{SO}} = -0.5t$, (c) $t_1 = t, \lambda_{\text{SO}} = t$, (d) $t_1 = t, \lambda_{\text{SO}} = 0$, (e) $t_1 = 3t, \lambda_{\text{SO}} = -0.4t$, (f) $t_1 = -3t, \lambda_{\text{SO}} = 0.4t$, (g) $t_1 = 3.2t, \lambda_{\text{SO}} = -0.2t$, (h) $t_1 = t, \lambda_{\text{SO}} = 0.2t$, (i) $t_1 = t, \lambda_{\text{SO}} = -0.2t$, (j) $t_1 = -t, \lambda_{\text{SO}} = 0.2t$, (k) $t_1 = 2.5t, \lambda_{\text{SO}} = -0.2t$, and (l) $t_1 = 0.5t, \lambda_{\text{SO}} = 0$.

acts as $\mathcal{P}[\psi_1(\mathbf{r}), \psi_2(\mathbf{r}), \psi_3(\mathbf{r}), \psi_4(\mathbf{r}), \psi_5(\mathbf{r}), \psi_6(\mathbf{r})]^T = [\psi_6(-\mathbf{r}), \psi_4(-\mathbf{r}), \psi_5(-\mathbf{r}), \psi_2(-\mathbf{r}), \psi_3(-\mathbf{r}), \psi_1(-\mathbf{r})]^T$, where $[\psi_1(\mathbf{r}), \psi_2(\mathbf{r}), \psi_3(\mathbf{r}), \psi_4(\mathbf{r}), \psi_5(\mathbf{r}), \psi_6(\mathbf{r})]^T$ is the six-component wave function. Taking Fourier transformation, we can write the six-component wave function as $[\psi_1(\mathbf{r}), \psi_2(\mathbf{r}), \psi_3(\mathbf{r}), \psi_4(\mathbf{r}), \psi_5(\mathbf{r}), \psi_6(\mathbf{r})]^T = \sum_{\mathbf{k}} [\phi_1(\mathbf{k}), \phi_2(\mathbf{k}), \phi_3(\mathbf{k}), \phi_4(\mathbf{k}), \phi_5(\mathbf{k}), \phi_6(\mathbf{k})] e^{i\mathbf{k}\cdot\mathbf{r}}$ and the parity operator as $\mathcal{P} = \sum_{\mathbf{k}} e^{i\mathbf{k}\cdot\mathbf{r}} \mathcal{P}_{\mathbf{k}} e^{-i\mathbf{k}\cdot\mathbf{r}}$. Then, in momentum space, we obtain the equation $\mathcal{P}_{\mathbf{k}}[\phi_1(\mathbf{k}), \phi_2(\mathbf{k}), \phi_3(\mathbf{k}), \phi_4(\mathbf{k}), \phi_5(\mathbf{k}), \phi_6(\mathbf{k})]^T = [\phi_6(-\mathbf{k}), \phi_4(-\mathbf{k}), \phi_5(-\mathbf{k}), \phi_2(-\mathbf{k}), \phi_3(-\mathbf{k}), \phi_1(-\mathbf{k})]^T$. Considering the degree of spin, we can express the parity

operator at the time reversal invariant momenta $\Gamma_{n_1 n_2 n_3}$ as follows,

$$\mathcal{P}_{\Gamma_{n_1 n_2 n_3}} = \begin{pmatrix} 1 & 0 \\ 0 & 1 \end{pmatrix} \otimes \begin{pmatrix} 0 & 0 & 0 & 0 & 0 & 1 \\ 0 & 0 & 0 & 1 & 0 & 0 \\ 0 & 0 & 0 & 0 & 1 & 0 \\ 0 & 1 & 0 & 0 & 0 & 0 \\ 0 & 0 & 1 & 0 & 0 & 0 \\ 1 & 0 & 0 & 0 & 0 & 0 \end{pmatrix} \quad (3)$$

where the 4×4 matrix is the unit matrix in spin space.

We diagonalize the total single-particle Hamiltonian $\mathcal{H}_{\mathbf{k}}$ and calculate the Z_2 topological invariants for different filling fractions. We find that non-trivial topological insulators exist for 1/6, 1/2 and 2/3 filling while only metal phase occurs for 1/3 and 5/6 filling. Thus, we will focus on and discuss the cases with 1/6, 1/2 and 2/3 filling fractions in the following part of the paper. We identify phases for different parameters t_1 and λ_{SO} with 1/6, 1/2 and 2/3 filling fractions and draw phase diagrams as shown in Fig.2. Figs.2(a), 2(b) and 2(c) show the phase diagrams for 1/6, 1/2 and 2/3 filling, respectively. For 1/6 and 2/3 filling, there are (1;111) and (1;000) STI phases, (0;111) WTI phase as well as trivial band insulator and metal phases. For 1/2 filling, there are (1;111) and (1;000) STI phases, trivial band insulator and metal phases except (0;111) WTI phase.

To clearly manifest the bulk band structure of different phases for various filling fractions, we calculate the bulk energy bands for several cases with different parameters t_1 and λ_{SO} , which are shown in Fig.3. In order to investigate the characteristics of surface states for various phases, we evaluate the energy bands in a slab geometry with two 001 surfaces. The Brillouin zone of the slab is shown in Fig.1(d). The energy bands are present along lines that connect the four surface TRIM as shown in Fig.4. With the assistance of the bulk energy bands shown in Fig.3 and the two-dimensional energy bands for a slab shown in Fig.4, we will sequentially analyze various phases, identify three-dimensional topological insulators, and discuss their characteristics for 1/6, 1/2 and 2/3 filling.

A. 1/6 filling

Fig.2(a) shows the phase diagram of the octahedron-decorated cubic lattice for 1/6 filling. In this case, the (1;111) and (1;000) STI phases are discovered. The non-trivial STI phases have a gap between the first and second bands as shown in Fig.3(a) and 3(b) corresponding to (1;111) and (1;000) STI phases, respectively. We note that for 1/6 filling there is only one Dirac point on TRIM as shown in Fig.4(a) and (b), that is, only a pair of robust spin-filtered states exists. We also find a (0;111) WTI phase for 1/6 filling e.g., as shown in Fig.3(c). Fig.4(c) shows the surface states for a (0;111) WTI phase that has two Dirac points between the first and second bands on TRIM. We note that trivial band insulators occur for

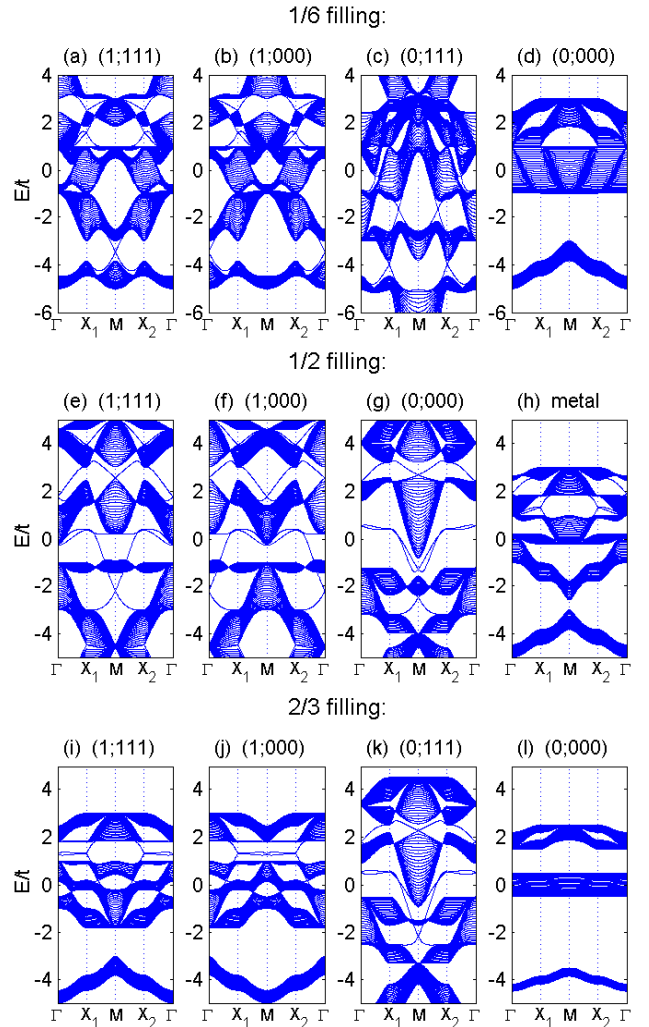


FIG. 4: (Color online). Band structures of a slab with two 001 surfaces for various parameters t_1 and λ_{SO} . Here, the horizontal axis represents the wave vectors along the path in the surface Brillouin zone indicated by the red lines in Fig.1(d). (a) $t_1 = t, \lambda_{\text{SO}} = 0.5t$, (b) $t_1 = -t, \lambda_{\text{SO}} = -0.5t$, (c) $t_1 = t, \lambda_{\text{SO}} = t$, (d) $t_1 = t, \lambda_{\text{SO}} = 0$, (e) $t_1 = 3t, \lambda_{\text{SO}} = -0.4t$, (f) $t_1 = -3t, \lambda_{\text{SO}} = 0.4t$, (g) $t_1 = 3.2t, \lambda_{\text{SO}} = -0.2t$, (h) $t_1 = t, \lambda_{\text{SO}} = 0.2t$, (i) $t_1 = t, \lambda_{\text{SO}} = -0.2t$, (j) $t_1 = -t, \lambda_{\text{SO}} = 0.2t$, (k) $t_1 = 2.5t, \lambda_{\text{SO}} = -0.2t$, and (l) $t_1 = 0.5t, \lambda_{\text{SO}} = 0$.

smaller t_1 and smaller λ_{SO} parameters, which is easily understood for when t_1 and λ_{SO} approaches to zero the lattice becomes separated octahedral clusters. For a trivial band insulator there is a gap between the first and second bands as shown in Fig.3(d), but there are not surface states as shown in Fig.4(d). For a metal phase, the gap vanishes.

B. 1/2 filling

Fig.2(b) shows the phase diagram of the octahedron-decorated cubic lattice for 1/2 filling. For 1/2 filling, (1;111) and (1;000) STI phases, trivial band insulators, and metal phases occur, but WTI phases are not found. Figs.3(e) and 3(f) show the band structure for (1;111) and (0;111) STI phases, respectively. We can find from these diagrams that a gap opens between the third and fourth bands. For STI phases, there only one Dirac point on TRIM as shown in Fig.4(e) and (f). For trivial band insulators, there is also a gap between the third and fourth bands as shown in Fig.3(g), but even number of Dirac points exist on TRIM as shown in Fig.4(g). For smaller t_1 and smaller λ_{SO} , a metal phase occurs except a special point $t_1 = 0$ and $\lambda_{SO} = 0$. For $t_1 = 0$ and $\lambda_{SO} = 0$, the second, third and fourth bands are degenerate and become a flat band, which means that electrons are localized. In other works, the system with t_1 and λ_{SO} for 1/2 filling is a trivial band insulator. However, a tiny change from $t_1 = 0$ and $\lambda_{SO} = 0$ for parameters t_1 and λ_{SO} makes the flat band become three dispersive bands that are crossover each other, then the lattice with three bands occupied becomes a metal.

C. 2/3 filling

Fig.2(c) shows the phase diagram of the octahedron-decorated cubic lattice for 2/3 filling. We note that, similar to 1/6 filling, (1;111) and (1;000) STI phases, (0;111) WTI phase, trivial band insulator, and metal phase occur in different ranges of parameters t_1 and λ_{SO} . Fig.3(i) shows the band structure for $t_1 = t, \lambda_{SO} = -0.2t$ at which a (1;111) STI phase occurs. We can find that a gap opens between the fourth and fifth bands as shown in Fig.3(i). There is an odd number of surface states which traverse the gap as shown in Fig.4(i). For the (1;000) STI phase, the similar characteristics are exemplified in Figs.3(j) and 4(j). The (0;111) WTI phase is found as

well. Fig.3(k) and Fig.4(k) show the (0;111) WTI phase has a gap between the fourth and fifth bands and an even number of surface states traversing the gap. For smaller t_1 and smaller λ_{SO} , the system for 2/3 filling is a trivial band insulator, which is feathered by a gap between the fourth and fifth bands combined with an even number of surface states traversing the gap as shown in Fig.3(l) and Fig.4(l), respectively.

IV. CONCLUSION

In summary, we have shown that the octahedron-decorated cubic lattice with spin-orbit coupling supports three-dimensional topological insulators at 1/6, 1/2 and 2/3 filling fractions. For 1/6 and 2/3 filling, (1;111) and (1;000) STI phases, (0;111) WTI phase, trivial band insulator, and metal phase are found, while for 1/2 filling, (1;111) and (1;000) STI phases, trivial band insulator, and metal phase occur except (0;111) WTI phase. We have calculated the band structure and surface band structure for the tight-binding model of the octahedron-decorated cubic lattice with spin-orbit coupling and evaluated the Z_2 topological invariants. We have analyzed and discussed the characters of the band structures and the surface states of different phases. Although the octahedron-decorated cubic lattice we considered is a toy model, our study points out an alternative path to search for real topological materials. On the other hand, it might as well be built from optical lattices due to their diversity and controllability.

Acknowledgments

This work was supported by the National Natural Science Foundation of China under Grant No. 11004028 and the Science and Technology Foundation of Southeast University under Grant No. KJ2010417

-
- [1] L. D. Landau, Phys. Z. Sowjetunion **11**, 26 (1937).
 - [2] K. v. Klitzing, G. Dorda, and M. Pepper, Phys. Rev. Lett. **45**, 494 (1980).
 - [3] D. J. Thouless, M. Kohmoto, M. P. Nightingale, and M. den Nijs, Phys. Rev. Lett. **49**, 405 (1982).
 - [4] F. D. M. Haldane, Phys. Rev. Lett. **61**, 2015 (1988).
 - [5] B. A. Bernevig and S. C. Zhang, Phys. Rev. Lett. **96**, 106802 (2006).
 - [6] C. L. Kane and E. J. Mele, Phys. Rev. Lett. **95**, 226801 (2005).
 - [7] C. L. Kane and E. J. Mele, Phys. Rev. Lett. **95**, 146802 (2005).
 - [8] B. A. Bernevig, T. L. Hughes, and S. C. Zhang, Science, **314**, 1757 (2006).
 - [9] M. König, S. Wiedmann, C. Brüne, *et al.*, Science **318**, 766 (2007).
 - [10] L. Fu, C. L. Kane, and E. J. Mele, Phys. Rev. Lett. **98**, 106803 (2007).
 - [11] J. E. Moore and L. Balents, Phys. Rev. B **75**, 121306 (2007).
 - [12] R. Roy, Phys. Rev. B **79**, 195322 (2009).
 - [13] L. Fu and C. L. Kane, Phys. Rev. B **76**, 045302 (2007).
 - [14] D. Hsieh, D. Qian, L. Wray, *et al.* Nature **542**, 970 (2008).
 - [15] Y. Xia, D. Qian, D. Hsieh, *et al.*, Nature Phys. **5**, 398 (2009).
 - [16] H. Zhang, C. X. Liu, X. L. Qi, *et al.*, Nature Phys. **5**, 438 (2009).
 - [17] Y. L. Chen, J. G. Analytis, J. H. Chu, *et al.*, Science **325**, 178 (2009).

- [18] D. Hsieh, Y. Xia, D. Qian, *et al.*, Nature **460**, 1101 (2009).
- [19] D. Hsieh, Y. Xia, D. Qian, *et al.*, Phys. Rev. Lett. **103** 146401 (2009).
- [20] H. M. Guo and M. Franz, Phys. Rev. B **80**, 113102 (2009).
- [21] K. Sun, H. Yao, E. Fradkin, and S. A. Kivelson, Phys. Rev. Lett. **103**, 046811 (2009).
- [22] A. Rüegg, J. Wen, and G. A. Fiete, Phys. Rev. B **81**, 205115 (2010).
- [23] C. Weeks and M. Franz, Phys. Rev. B **82**, 085310 (2010).
- [24] M. Kargarian and G. A. Fiete, Phys. Rev. B **82**, 085106 (2010).
- [25] H. M. Guo and M. Franz, Phys. Rev. Lett. **103**, 206805 (2009).